PM10 microplastics in indoor air: assessment of human exposure by inhalation in residential and car cabin environments

Nadiia Yakovenko, Théo Segur, Oskar Hagelskjaer, Henar Margenat, Gaël Le Roux, Jeroen E Sonke

PM_{10} microplastics in indoor air: assessment of human exposure by inhalation in residential and car cabin environments

Nadiia Yakovenko[*$†], Lucía Pérez-Serrano*[$†], Théo Segur*[†], Oskar Hagelskjaer*[†,‡], Henar Margenat*[‡], Gaël Le Roux*[‡], Jeroen E. Sonke*[*†]

[†] Géosciences Environnement Toulouse (GET), CNRS UMR5563 - IRD UR 234, Université Toulouse III - Paul Sabatier (UT3), 14 Avenue Edouard Belin, 31400 Toulouse, France.

[‡] Centre de Recherche sur la Biodiversité et l'Environnement (CRBE), Université de Toulouse, CNRS UMR 5300, IRD, Toulouse INP, Université Toulouse III – Paul Sabatier (UT3), 31326 Auzeville-Tolosane, France.

[$] These authors contributed equally

* Corresponding authors: nadiia.yakovenko@get.omp.eu, jeroen.sonke@get.omp.eu

ABSTRACT

The ubiquitous presence of airborne microplastics (MPs) in different indoor environments prompts serious concerns about the degree to which we inhale these particles and their potential impact on human health. Previous studies have mostly targeted MP in the 20–200 µm size range, which do

not penetrate into the lungs. In this study, we specifically investigate airborne, indoor suspended MPs in the inhalable 1–10 µm ($MP_{1–10µm}$) range in residential and car cabin environments, by using Raman spectroscopy. The median concentration of total suspended indoor MPs for the residential environment was 523 MPs/m^3 and 2,238 MPs/m^3 in the car cabin environment. The predominant polymer type in the residential environment was polyethylene (PE), and polyamide (PA) in the car cabin environment. Fragments were the dominant shape for 97% of the analyzed MPs, and 94% of MPs were smaller than 10 µm ($MP_{1–10µm}$), following a power size distribution law. We combine the new $MP_{1-10µm}$ observations with published indoor MP data to derive a consensus indoor MP concentration distribution, which we use to estimate human adult indoor MP inhalation of 3,900 MPs/day for the 10–300 µm ($MP_{10–300\ µm}$) range, and 68,000 MPs/day for $MP_{1–10µm}$. These exposure estimates are 100-fold higher than previous extrapolated estimates. We use the observed MP size distribution to estimate adult nanoplastic (NP) inhalation for 0.1–1 µm ($NP_{0.1–1µm}$) and 0.01–0.1 µm ($NP_{0.01–0.1µm}$) size ranges, at 1,500,000 and 33,000,000 NPs/day.

KEYWORDS: Raman, spectroscopy, plastic, pollution, inhalation

SYNOPSIS

This research reveals a high concentration of suspended indoor microplastic in the inhalable PM_{10} size range, emphasizing the potential health risks associated with human exposure to microplastic by inhalation.

Introduction

Microplastic (MP) is a ubiquitous pollutant resulting from the global extensive human use of plastic materials since 1950 and the mismanagement of plastic waste[1]. The term “microplastic”

refers to plastic particles between 1 μm and 5 mm in size that come in a variety of shapes, and polymer compositions, and can be classified by origin as primary (intentionally manufactured MPs) or secondary (MPs generated by the unintentional fragmentation of larger plastic items)[2–4]. Over the past decade, MPs have been detected in outdoor atmospheric aerosols[5–8] and deposition[9–14], in various parts of the world, from urban and highly industrialized areas[9,13] to remote mountainous regions[10,12], and the marine boundary layer[7]. The ubiquitous presence of MPs in the atmosphere raises many concerns about whether, and to what extent, we are inhaling MPs from outdoor and indoor air, with the latter likely playing the most significant role in human exposure to MPs through inhalation. Recent studies have shown that the concentration of indoor suspended MPs is eight times higher than outdoors[15], and the concentration of indoor deposited MP dust is 30 times higher than outdoors[16]. Given these findings, and the fact that people spend 90% of their time indoors[17–20], the greater potential for exposure to MPs through inhalation in indoor environments should be emphasized.

Airborne MPs differ in size, shape, and chemical composition, which determine the mechanism of their interaction with the respiratory system and the nature of potential negative effects. Inhaled particles larger than 10 μm are retained in the upper respiratory tract and undergo mucociliary clearance, while particles smaller than 10 μm can penetrate deeper into the lungs. The latter belong to the category of respirable particulate matter (PM) and are usually divided into two categories: PM_{10} (MPs < 10 μm) and $PM_{2.5}$ (MPs < 2.5 μm), which can cause respiratory problems like inflammation and chronic conditions such as bronchitis and asthma[21]. Additionally, MPs can carry toxic additives and adsorbed environmental pollutants, that may disrupt endocrine functions and increase risk of various diseases including cancer[22]. This combination of physical and chemical stressors makes MP inhalation a significant public health concern. Therefore, the assessment of

human exposure levels is extremely important but remains very challenging due to the novelty of the topic and need for specialized equipment and methods for indoor MP analysis. To date, one of the most commonly employed methods for analyzing indoor MPs is micro-Fourier Transform Infrared (μFTIR) spectroscopy[23]. The μFTIR has a limit of detection (LOD) of 10-20μm[23,24], and therefore mostly identifies larger MP that do not enter the lungs. In order to obtain accurate estimates of inhalation exposure to MPs and to conduct reliable risk assessments for humans, measurements of airborne MP in the PM_{10} range are required[25]. Raman spectroscopy (LOD 1μm) is highly effective for targeting smaller particles, making it a valuable tool for detecting MPs in various environments. However, despite its potential, only two studies[26,27] have applied it specifically to indoor suspended PM_{10} MPs. This indicates a significant gap in current research, as more data needs to be collected to achieve a comprehensive understanding of the abundance, sources, and behavior of PM_{10} MPs in indoor air. In this work we therefore performed quantitative and qualitative Raman analysis of suspended indoor MPs down to 1μm in residential and car cabin environments. MP concentrations in indoor air (MPs/m^3) were calculated and used to estimate human inhalation exposure (MPs/capita/unit time).

Material and Methods

Studied indoor environments

Two types of indoor environments were investigated in this study: a residential environment and a car cabin environment. The residential environment is represented by three apartments (seven samples) located in different parts of the city of Toulouse (France). The car cabin environment is represented by two different cars, from which five samples were collected while driving between the cities of Toulouse and Sigean, Toulouse and Grenoble, as well as within the

city of Marseille (all in France). Samples were collected between January and May 2023. Sampling details are summarized in **Table S1**.

Sampling of suspended indoor MPs

Indoor suspended MPs were collected through active sampling using KNF 12 and 220 V vacuum pumps. The aerosol collection system consisted of a 47 mm PFA Teflon filter holder (Savillex Corp.), with which air was collected through a 10 mm inlet and filtered through PTFE filters (Ø = 47 mm, pore size = 1 μm). The system was coupled with a gas volume meter to measure the sampled air volume. For sampling in the residential environment, the filter holders were placed horizontally at a height of 1.6–1.7 m from the floor, corresponding to the average human inhalation height[15]. Depending on the volume of collected air (V_{air}), the samples were divided into two groups: low-volume samples ($V_{air} < 3$ m^3) and high-volume samples ($V_{air} \geq 3$ m^3) (**Table S1**). No human activity was carried out during sampling in the apartments. Sampling in cars was carried out while driving the car with the windows closed. The in-car sampler was battery-powered and the filter holder was attached to the back of the front seat head rest. All samples were prepared in pre-cleaned individual filter holders under a class 100 laminar flow hood and wrapped in aluminum foil before and after deployment.

MP extraction prior to analysis

Particles from the low volume samples were directly transferred from the PTFE filter to the Anodisc aluminum oxide membrane filter (Ø = 25 mm, 0.22 μm pore size) without any pretreatment steps. Each PTFE filter was placed in a beaker containing 60 ml of 10% v/v methanol solution and sonicated for 10 min to detach particles from the filter surface. After that, the obtained suspension with the extracted particles was filtered onto an Anodisc filter. To minimize particle

loss during transfer, PTFE filter, beaker and the walls of the glass filtration unit were rinsed 3 times with 10% v/v methanol solution into the filtration unit. The Anodisc filter was then placed in a glass petri dish and dried overnight under a class 100 laminar flow hood before analysis.

Particle extraction from high volume samples included a density separation step aimed at removing inorganic matter that could potentially overlap the MPs on the filter. Density separation was performed using a calcium chloride ($CaCl_2$) solution with a density of 1.4 g/cm^3. Sufficient density separation required 7 days and was initiated by transferring particles from the PTFE filter to the $CaCl_2$ solution by sonicating the filter three times (t = 5 min) in $CaCl_2$ solution (50 mL). Every two days, the settled particles were removed from the density separation funnel. To maintain the volume constant, a new $CaCl_2$ solution was then added to the funnel, which was subsequently shaken to mix the contents and allow further particles to settle. After density separation, the samples were filtered onto an Anodisc filter and extensively rinsed with ultrapure Milli-Q water (18.2 MΩ·cm) to avoid $CaCl_2$ precipitation and then rinsed three times with ethanol. Identical to low volume samples, the obtained Anodisc filter was dried and stored in the glass petri dish prior to analysis.

Raman spectroscopy: Morphological and Chemical characterization

Raman analysis was conducted at a controlled room temperature (22ºC) using a Horiba (Jobin Yvon, France) LabRAM Soleil equipped with a high stability air-cooled He–Cd 532 nm laser diode and Nikon LV-NUd5 100x objective. The laser power was set to 6.3% (5.7 mW). Spectra were collected in the 200–3600 cm^{-1} range using 600 grooves/cm grating with a 100 µm split. The spectra acquisition time was set to 3s with 3x accumulation.

The Raman analysis was performed using automated particle identification (ParticleFinder module in the LabSpec 6 (LS6) software package). A high-resolution visual image of the 1 mm^2 filter area analyzed was acquired via the ViewSharp module, using a ±50 µm scan range to focus, and then converted into an 8-bit 0–255 greyscale image in the ParticleFinder module, where contrast parameters are set by the user to visually separate particles from the filter background. After setting all the parameters, the Raman spectra of each particle are collected one by one. In addition to chemical spectra, the ParticleFinder provides information on the particle location and morphological characteristics such as particle size, area, perimeter.

Raw spectra were processed and analyzed using the Spectragryph spectral analysis software V1.2.17d (Dr. Friedrich Menges SoftwareEntwicklung, www.effemm2.de/spectragryph). All spectra were subjected to adaptive baseline correction with a coarseness setting of 15%. Corrected spectra were cross-referenced, using our in-house library, which consists of selected spectra from SLoPP and SLoPP-E[28] and in-house spectra for Polymer Kit 1.0 (Hawaii Pacific University Center for Marine Debris Research: https://www.hpu.edu/cncs/cmdr) as well as plastic collected in the environment. Spectra were considered identified if the spectral hit quality index (HQI) values were higher than the threshold value set for each polymer type (**Table S2**).

For feasibility reasons, 0.3% (1 mm^2; 4,000 spectra; t = 14h) of the total effective area, excluding the outer polypropylene (PP) ring, (283.5 mm^2, Ø = 19 mm) of the Anodisc filter was analyzed. The analyzed area corresponds to the center of the filter membrane for all the samples, ensuring that analyses of different samples are consistent and results are comparable and reproducible.

Quality assurance and quality control (QA/QC)

Positive control. For positive controls, red polyethylene (R-PE) beads (Cospheric: https://www.cospheric.com/) of size 10–27 μm were used. Dry R-PE beads were dispersed in a Milli-Q water solution with 1% v/v Tween 20 for better particle dispersion. The positive control samples were spiked with 1–3 mL of R-PE solution (260 ± 36 particles/mL), and tests were performed to evaluate the particle recovery rate through extraction processes, as well as the homogeneity of particle distribution on the Anodisc filter.

MPs recovery rate. To assess the recovery rate of the applied protocols, spiked filter samples (n = 3) were optically imaged using the 10x objective of the Raman microscope (50 image mosaic, 2h) and the number of R-PE was counted in the ClickMaster2000 (https://www.thregr.org/wavexx/software/clickmaster2000/) software. Then, spiked samples underwent the same processing steps as real samples. The recovery rate (%) was calculated as the ratio between the number of particles found on the Anodisc filter and the initial number of spiked R-PE:

$$Recovery\ (\%) = \left(\frac{N_{recovered}}{N_{spiked}}\right) x\ 100 \quad (1)$$

Where $N_{recovered}$ is the final number of particles obtained after all processing steps, and N_{spike} is the initial number of R-PE that were counted on the unprocessed, spiked filters. Recovery rates of 81 ± 3% were observed (n = 5).

MP distribution on the filter. The spatial distribution of the spiked R-PE on the Anodisc filter was determined by analyzing their distribution pattern from the center to the edges of the filter. The Anodisc filter effective area (283.5 mm^2) was divided into four concentric rings (bins) (with mean distances from the center at 1.25, 3.75, 6.25, and 8.5 mm), and for each of these rings, particle

density (MPs/mm^2) was determined. The R-PE densities were plotted against the radial distance from the center of the filter (**Figure S1**).

Contamination control. All sample processing steps were performed under a class 100 laminar flow hood to avoid sample contamination. Operators were equipped with 100% cotton lab coats and nitrile gloves. All sampling tools were made of glass, metal or fluoropolymers (PTFE, PFA) to prevent contact with commodity plastics. Utensils (beakers, petri dishes, filtration units, and density separation funnels) were rinsed with abundant tap water, Milli-Q and ethanol. All glass tools were oven-cleaned before use, for 2 hours at 530°C. All reagents used (Milli-Q, ethanol, methanol and $CaCl_2$ solutions) were filtered through 1.0 µm PTFE and stored in Pyrex bottles (1L) with PTFE screw caps. The squeeze bottles used for Milli-Q and ethanol were made from perfluoroalkoxy alkanes (PFA). All filters were washed with Milli-Q and ethanol on both sides before use for sampling or transfer and manipulated with metal tweezers, which have been cleaned as formerly described. In addition, negative controls (blanks) were generated during sampling and further processing steps to examine potential sample contamination. For the blanks, the PTFE filter was placed in the filter holder without pumping. Filter holders for sampling and their corresponding blank were prepared the same day. The blank filters underwent the same procedure as their corresponding samples.

Data analysis

To obtain the final concentration of MPs in the air, the obtained Raman data were subjected to the following steps:

1. *Blank correction*, where the number of particles in the samples was adjusted for possible contamination during sample preparation and processing. Polymers found in blanks were

subtracted from their corresponding samples based on chemical composition and diameter range (e.g., if the blank presented two particles reported as PE in a [1,2) µm diameter range, these particles were subtracted from the count of PE [1,2) µm class in the sample).

2. *Recovery correction* was performed to account for particle loss during the processing steps and aimed at avoiding overestimation:

$$N_{MP\_recovery\_corrected} = \frac{N_{MPs\_detected}}{recovery\ rate} \quad (2)$$

Where $N_{MPs\_detected}$ is the number of particles identified by Raman analysis and the recovery rate is the percentage of spiked R-PE recovered after all processing steps.

3. *MP number extrapolation to the filter area*. The number of MP particles from the analyzed area (1 mm^2) was extrapolated to the entire effective area of the filter (283.5 mm^2), following the results from the radial distribution test of R-PE particles across the filter surface (**Figure S1**). Because the radial R-PE distribution was constant, indicating homogeneous deposition over the filter, the MP number extrapolation was quasi-linear and proportional to the surface areas.

4. *MP indoor concentration* (MPs/m^3) was calculated by dividing the total number of MPs on the sample filter by the air volume pumped through the filter. The standard definition for fine particulate matter, PM_{10}, in mass units (e.g. µg/m^3) covers the entire 0 to 10 µm range. Observation of MP in the 1–10 µm range in abundance/m^3 units by microscopy, therefore does not strictly correspond to the full PM_{10} range and definition. We, therefore, report MP observations with the $MP_{10–300µm}$ and $MP_{1–10µm}$ notation, and NP estimates with the $NP_{0.1–1µm}$ and $NP_{0.01–0.1µm}$ notation.

5. *MP inhalation* was calculated by multiplying human inhalation rate (m^3/capita/day) by MP concentration in air (MPs/m^3). The calculations were based on recommended EU default inhalation rates for adults and children[29].

Results and Discussion

Raman analysis

The Raman analysis involves a two-step process. First, a high-quality optical image of the analyzed area is captured and sent to ParticleFinder™ (Horiba). Here the optical image is analyzed by contrast to identify all particles and the Raman spectra of each particle are collected. Micron-sized aerosols, including MP, typically follow a power law size distribution where $MP_{1\text{-}10\mu m}$ sized target particles are most abundant. The amount of time necessary for Raman analysis therefore increases as the target particle size decreases. For analysis of particles down to 1 μm we use a 100x high-magnification objective to obtain high-quality optical images. Consequently, capturing a 1mm^2 filter area with the 100x objective and ViewSharp™ (z focus) required capturing 315 optical images to build a mosaic, which takes about 2 hours. In addition to this, the time to collect spectra required 14 hours and on average 3618 spectra were collected per 1 mm^2 sample area. The estimated time required for a complete optical image of the analyzed filter (299 x 403 photos) is approximately 669 hours, without the time required to collect the spectra. This makes it impossible to analyze the full area of the filter with the conditions used. Thus, only 0.3% (1 mm^2) of the total effective area (283.5 mm^2) of the Anodisc filter was analyzed. The number of particles from this 0.3% filter analyzed was extrapolated to the total effective area of the filter based on the results obtained from the radial distribution test.

Radial particle distribution

The radial particle distribution of spiked samples (n = 5) with R-PE was determined by measuring the particle density (MPs/mm^2) across four concentric rings on the Anodisc filter (**Table S3, Figure S1)**. R-PE particles were observed to be homogeneously distributed over the filter surface (one-way ANOVA; p-value = 0.55). The first concentric ring (d = 5mm; S = 19.6 mm^2) accounts for 7% of the filter surface area and 8 ± 3% of the total number of spiked R-PE. We assumed that sample MP processing yielded similar quasi-homogeneous radial MP distribution, and applied a particle number extrapolation to estimate the total number of MP on the filter. Radial distribution analysis is crucial when chemical analysis of particles is not possible on the entire filter surface and only a small area of the filter is analyzed. For example, tests (not shown here) using 1.0 µm PVDF filters, instead of Anodisc filter in the final step resulted in highly non-linear radial MP distributions.

Blank and recovery correction

In total, 12 samples and 4 corresponding blanks were analyzed. First, the number of particles from the 1mm^2 area analyzed for each sample was corrected for blank MP counts by subtracting the corresponding class of polymer and size range from the samples. Contamination accounted for 18% of the total number of particles identified. After blank correction, the number of particles was corrected for the recovery rate. MP recovery rate through the processing steps has been estimated at 81% (± 4) (n = 3) for a size range of 10–27 µm. Ideally, smaller spike MP should be used for $MP_{1–10µm}$ polymers but these were not available at the time of study. However, our previous size discriminating recovery analysis using MP fragments between 5-500 µm, did not result in a correlation between analytical recovery and particle size[30].

Indoor MP concentrations

Following blank correction and extrapolation of the results, the median concentration of total suspended MP from all indoor environments (concentrations in 12 samples) is 1,877 MPs/m^3 with an interquartile range (IQR), of 478 to 2,384 **(Figure 1, Table S4)**. Median residential suspended MP of 528 MPs/m^3 (IQR 288–2,487; n = 7) were lower than car cabin MP of 2,238 MPs/m^3 (IQR 1,515–2,245; n = 5), likely because of active ventilation inside cars. All residential sampling conditions represented low human activity conditions, except for sample MP15 which had high activity of two persons and resulted in the largest total MP concentration of 34,404 MPs/m^3.

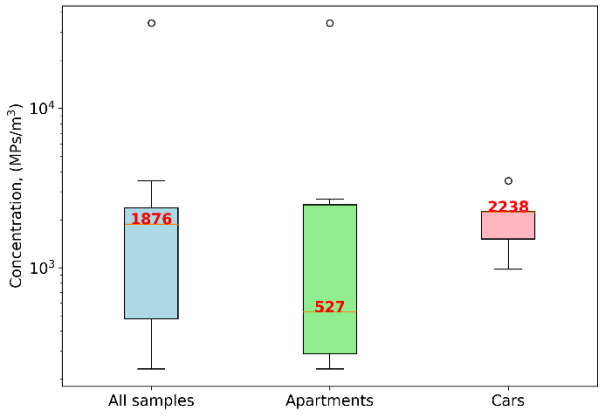

Figure 1. *Indoor total suspended MP concentration (MPs/m^3) for all samples (n = 12), apartments (n = 7), and cars (n = 5).*

Indoor MP composition

The polymer composition of MPs varies depending on the materials and objects that are an integral part of a certain indoor environment. In total, 10 different polymer types were identified in the environments studied (**Figure 2)** and Raman spectral matching is illustrated in **Figures S2-S10**. Suspended MPs in the investigated apartments were mainly composed of PE (76%) followed by polydimethylsiloxane (PDMS: 6.3%), PA (5.6%), PP (4.2%), polyethylene terephthalate (PET: 4.2%), polyhydroxybutyrate (PHB: 1.4%), polybutylene terephthalate (PBT: 1.4%), polystyrene

(PS: 0.7%) and acrylonitrile butadiene styrene (ABS: 0.7%). The widespread presence and high concentration of PE can be attributed to it being one of the most commonly produced and utilized polymers globally[31]. Additionally, PE is a low-density polymer with a density ranging from 0.91 to 0.98 g/cm³[32]. This lower density can potentially prolong its residence time in the air compared to high-density polymers. The obtained results are consistent with a similar study of suspended indoor MPs, where PE accounted for 74% [26], including in the $MP_{1–10\mu m}$ size fraction.

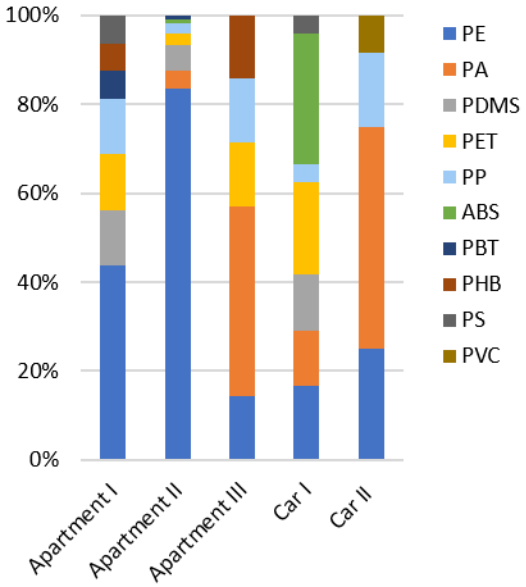

Figure 2. *Total suspended MP polymer composition observed in different indoor environments studied.*

The composition of polymers in cars differs from the composition of polymers in houses. In cars, the most common polymer was PA (25%), followed by ABS (19%), PE (19%), PET (14%), PP (8%), PDMS (8%), PS (3%) and polyvinyl chloride (PVC: 3%). PA, ABS, PE, PP and PVC are the main types of polymers used in car manufacturing [33]. We therefore suggest that wear and tear of vehicle interior parts made of plastic is a major source of MP exposure to drivers and passengers.

Indoor MP morphological characteristics

Shape

The analyzed MPs were defined as either fragments or fibers depending on their length-to-width (L/W) ratio. Particles with an L/W ratio > 3 were considered fibers, while particles with an L/W ratio ≤ 3 were classified as fragments[34]. Fragments accounted for 97% of the MPs represented by all 10 types of polymers identified in this study, and the remaining MP were fibers represented by PET, PA, and PP types. Recent studies show a tendency for fragments to dominate small suspended MPs in the air[34,15,26,27].

Size

The size of MPs in the residential environment was in the range of 1 to 28 μm and for the car cabin environment from 1 to 15 μm (**Figure 3**). The inhalable $MP_{1–10μm}$ fraction make up 94% of all detected MPs. MP abundances increase as the particle size decreases **(Figure 3)** and shows a typical power law distribution, $y = bx^{-\alpha}$. **Figure S11** summarizes published suspended MP size distributions (log size versus log % relative abundance), with a mean power law exponent of -1.65 ± 0.63 (1σ), that is typical of MP size distributions observed in a range of environments, with $\alpha = 1.6 \pm 0.5$ (n = 19)[35].

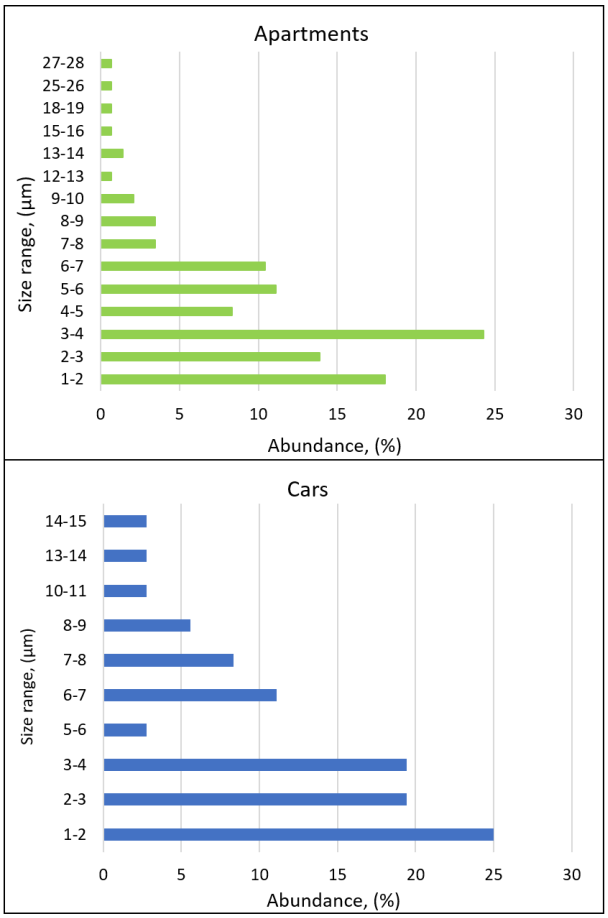

***Figure 3**. Observed indoor suspended MP size distribution in apartments (n = 7) and cars (n = 5).*

Comparison to literature

The presence of MPs in various environments, including households, offices, shopping centers, and public places[36,34,15,26,16,27], has been previously identified, demonstrating the ubiquitous presence of MPs in indoor air and indicating ongoing inhalation exposure. **Figure 4** compares the size distribution and indoor suspended MP concentrations from this study to published data. The higher concentration of MPs found in the current work is primarily due to the lower LOD (1 µm), which allows for the identification of more abundant smaller MP compared to FTIR studies with a higher LOD (10 µm)[9,34,37]. Maurizi et al. (2024), using Raman microscopy, reported average indoor MP concentrations ranging from 185 MPs/m³ in new to 548 MPs/m³ in older apartments.

These findings are consistent with our results for residential environment MP, which show a median concentration of 523 MPs/m³. Our study is the first to provide data on the presence of suspended MP in the car cabin environment, with a median concentration of 2,238 MPs/m³. Car MP concentrations were not significantly higher than apartment MP (Mann-Whitney U test; p-value = 0.5), due to the high variability in both environments.

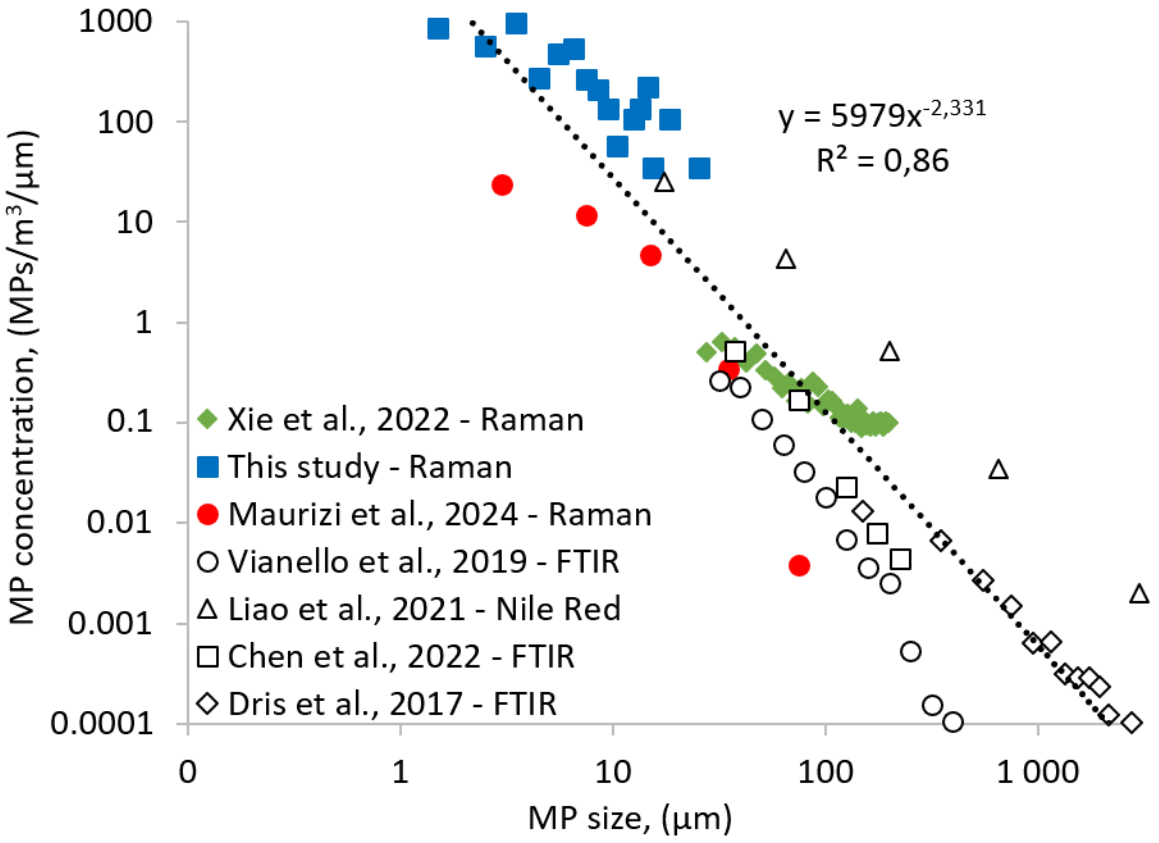

Figure 4. *Comparison of published indoor suspended MP concentrations in the 1 – 3000 µm range. FTIR microscopy typically probes MP > 20 µm, while Raman microscopy covers the* $MP_{1\text{-}10\mu m}$ *range down to 1 µm. The power law fit includes all data, except for select data points with low bias for small MP near the detection limits (inflected distributions from Vianello et al.*[34] *and Xie et al.*[26]*; see* ***Figure S11****). The MP concentration variability reflects both true environmental and method variability and shows an overall coherent estimate of human airborne MP exposure,*

described by the equation $y = 5979x^{-2,331}$ (r^2 of 0.86), and for standardized 1µm wide bins, meaning that the function returns the MP concentration in the 1-2µm range, for an x value of 1.5µm.

Published studies rarely include raw data, describing the size of each particle observed. To compare literature studies we therefore used the reported relative size distribution (percentage of MP, for a given size range, often 5 µm, 10 µm or larger size bins), and median MP concentrations (MPs/m^3), to reconstruct MP concentration distributions for standardized 1µm wide bins (e.g., 1–2 µm,…10–11 µm,…100–101 µm, etc.). It is important to compare different studies on the same number concentration scale, using identical size bins. Overall, the standardized data spread for all published suspended MP observations in **Figure 4** reflects the inherent power law distribution, the true environmental MP concentration differences, and the variability in methodology. Nevertheless, the different studies are highly complementary and define a power law size distribution with $y = 5979x^{-2,331}$ and r^2 of 0.86. We use the linearized form of the power law, $\log(y) = \alpha\log(x) + c$, with $\alpha = -2.331 \pm 0.098$ and $c = 3.776 \pm 0.204$ (1σ standard errors), and Monte Carlo simulation of 10,000 particle size distributions to derive uncertainty ranges for the indoor suspended MP concentration distribution in **Figure 4**. **Table 1** summarizes the key human exposure metrics based on **Figure 4**, suggesting we inhale indoor air that contains on average 240 ± 180 MP/m^3 in the 10-300 µm range, and 4,200 ± 2,200 MPs/m^3 in the 1–10 µm range. The new observation-based $MP_{1–10µm}$ concentration estimate of 4,200 MPs/m^3 exceeds a previous extrapolated (from FTIR data > 20 µm) estimate of 36 MPs/m^3 by two orders of magnitude but lies within the 95th percentile (19,000 MPs/m^3) of that study[38]. The new $MP_{1–10µm}$ estimate also exceeds our direct indoor $MP_{1–10µm}$ observation of 1,704 MPs/m^3 (**Table S4**), because the consensus power law in **Figure 4** has a higher MP abundance than our observations at the lower, 1–3 µm end of the $MP_{1–10µm}$ range. Observations of atmospheric nanoplastic (NP) particles and

MP in the same rainfall samples have been shown to extend the power law size distribution into the NP regime < 450 nm[39]. We therefore extrapolate the power law in **Figure 4** to provide approximate estimates of potential human NP exposure by inhalation of 1,500,000 ± 850,000 NPs/m^3 in the 0.1–1.0 μm range, and 33,000,000 ± 21,000,000 NPs/m^3 in the 0.01–0.1 μm range. Indoor NP concentration observations are needed to verify these NP exposure estimates, especially because ultrafine particulate matter has a shorter atmospheric lifetime, leading to incorporation into larger aerosols or deposition to surfaces.

Inhalation rates

For the evaluation of human exposure through inhalation we use EU recommended default inhalation rates for two age groups including adults (31–51 years, 16 ± 4 m^3/day) and children (2–12 years, 11 ± 3 m^3/day)[29]. The estimated inhalation concentration for $MP_{10–300μm}$ is 2,700 ± 2,100 and 3,900 ± 3,100 MPs/day for children and adults, respectively. These particles do not penetrate the lungs, but are most likely subjected to mucociliary clearance[40]. Inhaled MPs trapped in the mucus layer are moved from the lower respiratory tract (bronchi and bronchioles) to the upper respiratory tract (throat). When mucus with trapped MPs reaches the throat, it can be coughed up or cleared by the body through expectoration (spitting) or swallowing[41]. The process of swallowing is the most likely way to evacuate the mucus, but it leads to the transport of MPs to the gastrointestinal system. The potential $MP_{10–300μm}$ intestinal intake, from airborne exposure, exceeds best-estimates of median dietary MP exposure of 553 and 858 MPs/day for children and adults in the 1–5000 μm range[38], suggesting that inhalation of $MP_{10–300μm}$ is an indirect pathway for MP exposure through inhalation, adding to the overall burden of MPs in the human body. The estimated inhalation of indoor suspended $MP_{1–10μm}$ is 47,000 ± 28,000 and 68,000 ± 40,000

370 MPs/day for children and adults, respectively (**Table 1**). Finally, the potential inhalation of indoor
371 suspended NP is 20 and 400-fold higher than for $MP_{1–10\mu m}$ (**Table 1**).

372 ***Table 1.*** *Estimates of indoor suspended MP fragment concentrations, based on all available*
373 *literature observations in the 1.0 - 300 µm range shown in* ***Figure 4*** *and fitted by the power law,*
374 $y = 5979x^{-2,331}$. *Suspended NP concentrations in the 0.1–1.0 µm and 0.01–0.1 µm range are based*
375 *on extrapolation of observed MP. Daily inhalation for children and adults is estimated based on*
376 *concentrations and inhalation rates of 11 ± 3 and 16 ± 4 m^3 per day respectively. All uncertainties*
377 *are 1σ standard deviations. MP mass concentrations in picogram per m^3 are estimated by*
378 *assuming a MP density of 1 g/cm^3, and an ellipsoidal MP fragment shape, and volume,*
379 *$V = 0.1 \times D^3$, where D is MP diameter.*

Size range	Concentration		Inhalation, (particles/day)	
	(particles/m^3)	(pg/m^3)	Children	Adults
$MP_{10–300\mu m}$	240 ± 200	2.0E+08	2,700 ± 2,100	3,900 ± 3,100
$MP_{1–10\mu m}$	4,300 ± 2,300	2.5E+02	47,000 ± 28,000	68,000 ± 40,000
$NP_{0.1–1\mu m}$	94,000 ± 48,000	2.5E-01	1,000,000 ± 600,000	1,500,000 ± 850,000
$NP_{0.01–0.1\mu m}$	2,100,000 ± 1,200,000	2.5E-10	23,000,000 ± 15,000,000	33,000,000 ± 21,000,000

380

381 In summary, our study documents that indoor suspended $MP_{1–10\mu m}$ concentrations are higher than
382 previously thought. Consequently, human inhalation of fine particulate $MP_{1–10\mu m}$, and likely NP,
383 that penetrate deep lung tissue may contribute to causing lung tissue damage, inflammation and
384 associated diseases. We also suggest that inhaled $MP_{10–300\mu m}$ removed by mucociliary clearance,
385 contributes to high intestinal MP intake.

386

AUTHOR INFORMATION

Corresponding authors: nadiia.yakovenko@get.omp.eu, jeroen.sonke@get.omp.eu

AUTHOR CONTRIBUTIONS

N. Yakovenko and L. Pérez Serrano contributed equally to this work, including the lab work, data acquisition and manuscript writing. N.Y. and J.S. designed the study. O.H., H.M. and G.L.R. assisted in the Raman microscopy method development. N.Y., J.S. and T.S. performed data treatment. N.Y., L.P.S. and J.S. wrote the manuscript and all authors provided critical comments.

ACKNOWLEDGMENT. We thank the reviewers for their constructive comments. We acknowledge financial support via the ANR-20-CE34-0014 ATMO-PLASTIC and ANR-23-CE34-0012 BUBBLPLAST grants, and a PhD scholarship from the French ministry of higher education and research.

REFERENCES

(1) Geyer, R.; Jambeck, J. R.; Law, K. L. Production, Use, and Fate of All Plastics Ever Made. *Sci. Adv.* **2017**, *3* (7), e1700782. https://doi.org/10.1126/sciadv.1700782.

(2) Thompson, R. C.; Olsen, Y.; Mitchell, R. P.; Davis, A.; Rowland, S. J.; John, A. W. G.; McGonigle, D.; Russell, A. E. Lost at Sea: Where Is All the Plastic? *Science* **2004**, *304* (5672), 838–838. https://doi.org/10.1126/science.1094559.

(3) Phuong, N. N.; Zalouk-Vergnoux, A.; Poirier, L.; Kamari, A.; Châtel, A.; Mouneyrac, C.; Lagarde, F. Is There Any Consistency between the Microplastics Found in the Field and Those Used in Laboratory Experiments? *Environ. Pollut.* **2016**, *211*, 111–123. https://doi.org/10.1016/j.envpol.2015.12.035.

(4) Cole, M.; Lindeque, P.; Halsband, C.; Galloway, T. S. Microplastics as Contaminants in the Marine Environment: A Review. *Mar. Pollut. Bull.* **2011**, *62* (12), 2588–2597. https://doi.org/10.1016/j.marpolbul.2011.09.025.

(5) Liu, K.; Wang, X.; Wei, N.; Song, Z.; Li, D. Accurate Quantification and Transport Estimation of Suspended Atmospheric Microplastics in Megacities: Implications for Human Health. *Environ. Int.* **2019**, *132*, 105127. https://doi.org/10.1016/j.envint.2019.105127.

(6) Trainic, M.; Flores, J. M.; Pinkas, I.; Pedrotti, M. L.; Lombard, F.; Bourdin, G.; Gorsky, G.; Boss, E.; Rudich, Y.; Vardi, A. Airborne Microplastic Particles Detected in the Remote Marine Atmosphere. *Commun. Earth Environ.* **2020**, *1* (1), 1–9. https://doi.org/10.1038/s43247-020-00061-y.

(7) Wang, X.; Li, C.; Liu, K.; Zhu, L.; Song, Z.; Li, D. Atmospheric Microplastic over the South China Sea and East Indian Ocean: Abundance, Distribution and Source. *J. Hazard. Mater.* **2020**, *389*, 121846. https://doi.org/10.1016/j.jhazmat.2019.121846.

(8) González-Pleiter, M.; Edo, C.; Aguilera, Á.; Viúdez-Moreiras, D.; Pulido-Reyes, G.; González-Toril, E.; Osuna, S.; de Diego-Castilla, G.; Leganés, F.; Fernández-Piñas, F. Occurrence and Transport of Microplastics Sampled within and above the Planetary Boundary Layer. *Sci. Total Environ.* **2021**, *761*, 143213. https://doi.org/10.1016/j.scitotenv.2020.143213.

(9) Dris, R.; Gasperi, J.; Saad, M.; Mirande, C.; Tassin, B. Synthetic Fibers in Atmospheric Fallout: A Source of Microplastics in the Environment? *Mar. Pollut. Bull.* **2016**, *104* (1), 290–293. https://doi.org/10.1016/j.marpolbul.2016.01.006.

(10) Bergmann, M.; Mützel, S.; Primpke, S.; Tekman, M. B.; Trachsel, J.; Gerdts, G. White and Wonderful? Microplastics Prevail in Snow from the Alps to the Arctic. *Sci. Adv.* **2019**, *5* (8), eaax1157. https://doi.org/10.1126/sciadv.aax1157.

(11) Cai, L.; Wang, J.; Peng, J.; Tan, Z.; Zhan, Z.; Tan, X.; Chen, Q. Characteristic of Microplastics in the Atmospheric Fallout from Dongguan City, China: Preliminary Research and First Evidence. *Environ. Sci. Pollut. Res.* **2017**, *24* (32), 24928–24935. https://doi.org/10.1007/s11356-017-0116-x.

(12) Allen, S.; Allen, D.; Phoenix, V. R.; Le Roux, G.; Durántez Jiménez, P.; Simonneau, A.; Binet, S.; Galop, D. Atmospheric Transport and Deposition of Microplastics in a Remote Mountain Catchment. *Nat. Geosci.* **2019**, *12* (5), 339–344. https://doi.org/10.1038/s41561-019-0335-5.

(13) Klein, M.; Fischer, E. K. Microplastic Abundance in Atmospheric Deposition within the Metropolitan Area of Hamburg, Germany. *Sci. Total Environ.* **2019**, *685*, 96–103. https://doi.org/10.1016/j.scitotenv.2019.05.405.

(14) Materić, D.; Kasper-Giebl, A.; Kau, D.; Anten, M.; Greilinger, M.; Ludewig, E.; van Sebille, E.; Röckmann, T.; Holzinger, R. Micro- and Nanoplastics in Alpine Snow: A New Method for Chemical Identification and (Semi)Quantification in the Nanogram Range. *Environ. Sci. Technol.* **2020**, *54* (4), 2353–2359. https://doi.org/10.1021/acs.est.9b07540.

(15) Liao, Z.; Ji, X.; Ma, Y.; Lv, B.; Huang, W.; Zhu, X.; Fang, M.; Wang, Q.; Wang, X.; Dahlgren, R.; Shang, X. Airborne Microplastics in Indoor and Outdoor Environments of a Coastal City in Eastern China. *J. Hazard. Mater.* **2021**, *417*, 126007. https://doi.org/10.1016/j.jhazmat.2021.126007.

(16) Zhai, X.; Zheng, H.; Xu, Y.; Zhao, R.; Wang, W.; Guo, H. Characterization and Quantification of Microplastics in Indoor Environments. *Heliyon* **2023**, *9* (5), e15901. https://doi.org/10.1016/j.heliyon.2023.e15901.

(17) European Commission. *Indoor air pollution: new EU research reveals higher risks than previously thought*. https://ec.europa.eu/commission/presscorner/detail/en/IP_03_1278 (accessed 2024-08-18).

(18) Diffey, B. L. An Overview Analysis of the Time People Spend Outdoors. *Br. J. Dermatol.* **2011**, *164* (4), 848–854. https://doi.org/10.1111/j.1365-2133.2010.10165.x.

(19) Mannan, M.; Al-Ghamdi, S. G. Indoor Air Quality in Buildings: A Comprehensive Review on the Factors Influencing Air Pollution in Residential and Commercial Structure. *Int. J. Environ. Res. Public. Health* **2021**, *18* (6), 3276. https://doi.org/10.3390/ijerph18063276.

(20) US EPA, O. *Improving Your Indoor Environment*. https://www.epa.gov/indoor-air-quality-iaq/improving-your-indoor-environment (accessed 2024-08-14).

(21) Prata, J. C. Airborne Microplastics: Consequences to Human Health? *Environ. Pollut.* **2018**, *234*, 115–126. https://doi.org/10.1016/j.envpol.2017.11.043.
(22) Landrigan, P. J.; Raps, H.; Cropper, M.; Bald, C.; Brunner, M.; Canonizado, E. M.; Charles, D.; Chiles, T. C.; Donohue, M. J.; Enck, J.; Fenichel, P.; Fleming, L. E.; Ferrier-Pages, C.; Fordham, R.; Gozt, A.; Griffin, C.; Hahn, M. E.; Haryanto, B.; Hixson, R.; Ianelli, H.; James, B. D.; Kumar, P.; Laborde, A.; Law, K. L.; Martin, K.; Mu, J.; Mulders, Y.; Mustapha, A.; Niu, J.; Pahl, S.; Park, Y.; Pedrotti, M.-L.; Pitt, J. A.; Ruchirawat, M.; Seewoo, B. J.; Spring, M.; Stegeman, J. J.; Suk, W.; Symeonides, C.; Takada, H.; Thompson, R. C.; Vicini, A.; Wang, Z.; Whitman, E.; Wirth, D.; Wolff, M.; Yousuf, A. K.; Dunlop, S. The Minderoo-Monaco Commission on Plastics and Human Health. *Ann. Glob. Health* **2023**, *89* (1). https://doi.org/10.5334/aogh.4056.
(23) Noorimotlagh, Z.; Hopke, P. K.; Mirzaee, S. A. A Systematic Review of Airborne Microplastics Emissions as Emerging Contaminants in Outdoor and Indoor Air Environments. *Emerg. Contam.* **2024**, *10* (4), 100372. https://doi.org/10.1016/j.emcon.2024.100372.
(24) Huppertsberg, S.; Knepper, T. P. Validation of an FT-IR Microscopy Method for the Determination of Microplastic Particles in Surface Waters. *MethodsX* **2020**, *7*, 100874. https://doi.org/10.1016/j.mex.2020.100874.
(25) Wright, S. L.; Gouin, T.; Koelmans, A. A.; Scheuermann, L. Development of Screening Criteria for Microplastic Particles in Air and Atmospheric Deposition: Critical Review and Applicability towards Assessing Human Exposure. *Microplastics Nanoplastics* **2021**, *1* (1), 6. https://doi.org/10.1186/s43591-021-00006-y.
(26) Xie, Y.; Li, Y.; Feng, Y.; Cheng, W.; Wang, Y. Inhalable Microplastics Prevails in Air: Exploring the Size Detection Limit. *Environ. Int.* **2022**, *162*, 107151. https://doi.org/10.1016/j.envint.2022.107151.
(27) Maurizi, L.; Simon-Sánchez, L.; Vianello, A.; Nielsen, A. H.; Vollertsen, J. Every Breath You Take: High Concentration of Breathable Microplastics in Indoor Environments. *Chemosphere* **2024**, *361*, 142553. https://doi.org/10.1016/j.chemosphere.2024.142553.
(28) Munno, K.; De Frond, H.; O'Donnell, B.; Rochman, C. M. Increasing the Accessibility for Characterizing Microplastics: Introducing New Application-Based and Spectral Libraries of Plastic Particles (SLoPP and SLoPP-E). *Anal. Chem.* **2020**, *92* (3), 2443–2451. https://doi.org/10.1021/acs.analchem.9b03626.
(29) European Chemicals Agency. Default Human Factor Values for Use in Exposure Assessments for Biocidal Products, 2017. https://echa.europa.eu/documents/10162/21664016/recom_14+_default+human_factor_values_biocidal+products_en.pdf/88354d31-8a3a-475a-9c7d-d8ef8088d004.
(30) Hagelskjær, O.; Crézé, A.; Le Roux, G.; Sonke, J. E. Investigating the Correlation between Morphological Features of Microplastics (5–500 Mm) and Their Analytical Recovery. *Microplastics Nanoplastics* **2023**, *3* (1), 22. https://doi.org/10.1186/s43591-023-00071-5.
(31) Plastics Europe. *The Circular Economy for Plastics – A European Analysis 2024 • Plastics Europe*; 2024. https://plasticseurope.org/knowledge-hub/the-circular-economy-for-plastics-a-european-analysis-2024/ (accessed 2024-08-15).
(32) Pruitt, L. A. 1.122 - Structural Biomedical Polymers (Nondegradable). In *Comprehensive Biomaterials*; Ducheyne, P., Ed.; Elsevier: Oxford, 2011; pp 373–379. https://doi.org/10.1016/B978-0-08-055294-1.00036-2.

(33) Ortego, A.; Russo, S.; Iglesias-Émbil, M.; Valero, A.; Magdalena, R. Exergy Assessment of Plastic Car Parts. *Vehicles* **2023**, *5* (3), 1211–1226. https://doi.org/10.3390/vehicles5030067.
(34) Vianello, A.; Jensen, R. L.; Liu, L.; Vollertsen, J. Simulating Human Exposure to Indoor Airborne Microplastics Using a Breathing Thermal Manikin. *Sci. Rep.* **2019**, *9* (1), 1–11. https://doi.org/10.1038/s41598-019-45054-w.
(35) Kooi, M.; Koelmans, A. A. Simplifying Microplastic via Continuous Probability Distributions for Size, Shape, and Density. *Environ. Sci. Technol. Lett.* **2019**, *6* (9), 551–557. https://doi.org/10.1021/acs.estlett.9b00379.
(36) Dris, R.; Gasperi, J.; Mirande, C.; Mandin, C.; Guerrouache, M.; Langlois, V.; Tassin, B. A First Overview of Textile Fibers, Including Microplastics, in Indoor and Outdoor Environments. *Environ. Pollut.* **2017**, *221*, 453–458. https://doi.org/10.1016/j.envpol.2016.12.013.
(37) Chen, E.-Y.; Lin, K.-T.; Jung, C.-C.; Chang, C.-L.; Chen, C.-Y. Characteristics and Influencing Factors of Airborne Microplastics in Nail Salons. *Sci. Total Environ.* **2022**, *806*, 151472. https://doi.org/10.1016/j.scitotenv.2021.151472.
(38) Mohamed Nor, N. H.; Kooi, M.; Diepens, N. J.; Koelmans, A. A. Lifetime Accumulation of Microplastic in Children and Adults. *Environ. Sci. Technol.* **2021**, *55* (8), 5084–5096. https://doi.org/10.1021/acs.est.0c07384.
(39) Allen, S.; Materić, D.; Allen, D.; MacDonald, A.; Holzinger, R.; Roux, G. L.; Phoenix, V. R. An Early Comparison of Nano to Microplastic Mass in a Remote Catchment's Atmospheric Deposition. *J. Hazard. Mater. Adv.* **2022**, *7*, 100104. https://doi.org/10.1016/j.hazadv.2022.100104.
(40) Prata, J. C. Microplastics and Human Health: Integrating Pharmacokinetics. *Crit. Rev. Environ. Sci. Technol.* **2023**, *53* (16), 1489–1511. https://doi.org/10.1080/10643389.2023.2195798.
(41) Xu, L.; Jiang, Y. Mathematical Modeling of Mucociliary Clearance: A Mini-Review. *Cells* **2019**, *8* (7), 736. https://doi.org/10.3390/cells8070736.